STEADY RISE OF A LIQUID DROP IN A VISCOUS LIQUID

P. K. Volkov

UDC 532.529.6

1. Introduction. The rise of a liquid drop in a different medium is a very complicated problem because it is necessary to determine the hydrodynamic characteristics inside and outside the drop and also the drop shape, i.e., the interface between the two different media. The rise velocity depends significantly on the physical properties of the two media and also on the structure of the flow. Hence it is not as straightforward to transform to the equivalent (and usually simpler) problem of flow around a stationary drop as in the case of a motion of a drop with known shape and given velocity. The steady rise of a drop must therefore be distinguished from motion with a given constant velocity, such as motion of a solid body. As a simple example, a solid ball rises (sinks) in a liquid with a certain velocity and its motion can be determined for different values of the velocity. Then rise occurs for a certain value of the parameter characterizing motion of the body with a constant velocity. The situation becomes more complicated if the shape of the body can change as a result of the hydrodynamics of the process.

The mathematical description of the rise of a liquid drop in a different liquid is based on the solution of the Navier–Stokes equations inside and outside the drop subject to certain matching conditions on the boundary between the media. The earlier papers [1, 2] considered the solution in the Stokes approximation. In this case the drop is a sphere and a Hill vortex exists inside the drop. Deformation of a drop was studied theoretically in [3] in the Oseen approximation by matching asymptotic expansions. The shape of the drop was found to be almost spherical. Approximate solutions for large Reynolds numbers in the form of a series ofpolynomials were obtained in [4, 5] for spherical drops using the Bubnov–Galerkin method. Because the Navier–Stokes equations and the boundary conditions are nonlinear, a complete solution to the problem can be found only numerically. The direct numerical solution of the complete Navier–Stokes equations was considered in [6, 7] and the flow was determined for intermediate values of the hydrodynamic parameters. A more complete review of the literature is given in [8]. All of the theoretical solutions mentioned above are different asymptotic limits of small or large values of the hydrodynamic parameters, or else assume that the drop is only slightly deformable, or consider steady flow past the drop [6]. Hence the correspondence between these solutions and the original problem of the rise of a drop requires further study. For spherical drops this question is easily resolved (the flow is steady when the drag and buoyancy forces are equal), but for deformed drops the problem is more complicated. The steady rise of a drop in a vertical tube was solved in [9] using the algorithm for the numerical solution of the rise of a bubble in a viscous liquid. In the present paper we study the flow inside and outside the drop and its effect on the rise of a drop in an infinite liquid for intermediate values of the hydrodynamic parameters. The different flow regimes are discussed and the calculated results are compared with the limiting cases of a very viscous drop (a solid particle) and a bubble.

2. Statement of the Problem and Dimensional Analysis. A liquid drop of density ρ_1 and kinematic viscosity ν_1 moves in a liquid at rest with density ρ_2 and kinematic viscosity ν_2. The acceleration of gravity g is directed downward. If $\rho_1 = \rho_2$ the drop is in equilibrium, for $\rho_1 < \rho_2$ it rises, and for $\rho_1 > \rho_2$ it sinks. In any case one expects steady motion, since the buoyancy force and the drag force act in opposite directions. Since the volume of the drop is constant (and hence the buoyancy force is constant), eventually the drag force will become comparable in magnitude to the buoyancy force. If the shape of the drop and the nature of the flow do not change significantly, then we speak of steady rise (fall) with velocity **U**, which is determined by the entire process.

We assume rectangular coordinates (x_1, x_2, x_3) with the origin O in the external liquid. The Navier–Stokes equations can be written in the form

$$\partial \mathbf{u}_i/\partial t + \mathbf{u}_i \nabla \mathbf{u}_i + (1/\rho_i)\nabla(p_i + \rho_i g x_3) = \nu_i \Delta \mathbf{u}_i, \ \operatorname{div} \mathbf{u}_i = 0 \qquad (2.1)$$

Novosibirsk. Translated from Prikladnaya Mekhanika i Tekhnicheskaya Fizika, No. 1, pp. 78-88, January-February, 1992. Original article submitted July 12, 1990.

0021-8944/92/3301-0071$12.50

($i = 1, 2$ refers to the liquids inside and outside the drop, the $\mathbf{u}_i$ are the velocity vectors, and the p_i are the pressures).

The boundary conditions are specified as follows. On the surface Γ of the drop [$F(x_1, x_2, x_3, t) = 0$] the velocities and tangential stresses in the two liquids must be equal, while the difference in the normal stresses must be equal to the capillary pressure:

$$\mathbf{u}_1 = \mathbf{u}_2; \tag{2.2}$$

$$\rho_1\nu_1\tau S_1\mathbf{n} = \rho_2\nu_2\tau S_2\mathbf{n}; \tag{2.3}$$

$$p_1 - 2\rho_1\nu_1\mathbf{n}S_1\mathbf{n} - p_2 + 2\rho_2\nu_2\mathbf{n}S_2\mathbf{n} = \sigma K - p_{cap} + p_\infty. \tag{2.4}$$

Here σ is the surface tension on the interface; τ, $\mathbf{n}$ are unit vectors tangent and normal to Γ; $S_i^{kj} = (\partial u_i^k/\partial x_j + \partial u_i^j/\partial x_k)/2$ is the deformation rate tensor; K is the curvature of the surface Γ. The stress tensor is $T_i = -p_i I + 2\rho_i\nu_i S_i$. In addition, we must have the kinematic condition

$$\partial F/\partial t + \mathbf{u}_i\nabla F = 0. \tag{2.5}$$

At infinity the liquid is assumed to be at rest:

$$\mathbf{u}_2 \to 0 \text{ when } \mathbf{x} \to \infty. \tag{2.6}$$

The problem (2.1)-(2.6) is unsteady and describes the rise of the drop under the force of gravity. It is required to determine u_1, u_2, p_1, p_2, and F. In the limit of steady rise (if it exists) $\partial F/\partial t \to \text{const} = \mathbf{U}$ is the rise velocity of the drop.

The conditions (2.2) and (2.3) ensure the continuity of the velocities and tangential stresses across the interface; (2.4) implies that the discontinuity in the normal stress is equal to the capillary pressure. In equilibrium ($\rho_1 = \rho_2$ or $g = 0$) it follows from (2.4) that the surface is a sphere and the pressure p_{cap} inside the drop is not arbitrary, but is determined in terms of the radius a of the drop by (2.4), which takes the form

$$p_{cap} - p_\infty = 2\sigma/a. \tag{2.7}$$

It follows from (2.4) and (2.7) that the solution of the problem depends on the difference $(p_{cap} - p_\infty)$, where $(p_{cap} - p_\infty)$ and a are not independent if the two media are specified. Hence (2.1)-(2.6) involve seven independent dimensional parameters: ρ_1, ν_1, ρ_2, ν_2, σ, g, and a. It follows from dimensional analysis that the solution of (2.1)-(2.6) is determined by four independent dimensionless parameters.

3. Method of Solution. For steady-state motion (2.1)-(2.6) simplify and become independent of time in a coordinate system moving with the drop. In this coordinate system the drop is at rest and the liquid flows around it. At an infinite distance from the drop the velocity of the liquid is constant and equal to the rise velocity $\mathbf{U}$. The time derivatives vanish in (2.1) and (2.5). We consider the axisymmetric case. It is convenient to introduce spherical coordinates and to transform from the variables $\mathbf{u}_i$ and p_i to the stream functions ψ_i and vorticities ω_i. Then the number of unknown functions is reduced to four and we obtain four equations of the elliptic type for the functions ψ_1, ψ_2, ω_1, ω_2 and an ordinary differential equation for the boundary function F [9]. As mentioned above, the problem involves four independent dimensionless parameters. Different parameters are obtained, depending on the method used to make the original equations dimensionless. Taking a and $\mathbf{U}$ as the units of length and velocity, and transforming to dimensionless equations in the usual way [9, 10], we obtain $\mathrm{Re}_1 = \mathbf{U}2a/\nu_1$, $\mathrm{Re}_2 = \mathbf{U}2a/\nu_2$ (the Reynolds numbers of the internal and external flows), $\mathrm{We} = \rho_2\mathbf{U}^2 2a/\sigma$ (the Weber number), $\rho = \rho_1/\rho_2$ (the ratio of the densities), $\mathrm{Fr} = \mathbf{U}^2/ga$ (the Froude number), and $\mathrm{Pd} = (p_{cap} - p_\infty)2a/\sigma$.

The parameter ρ determines the process: the drop rises for $\rho < 1$ and sinks for $\rho > 1$; Re_1 and Re_2 characterize the hydrodynamic properties of the liquids; We corresponds to deformation of the surface; Fr and Pd must be determined simultaneously with the flow functions (as in [10], for example) from the conditions for steady flow and constancy of the volume of the drop.

In the present paper we assume $\rho = 0.1$ for two reasons. First, for certain values of Re_1 the results can be compared to calcualtions for a bubble [10, 11]. Second, this case is important in itself as it models the rise of gas bubbles. When We = 0 the condition (2.4) gives $K = \mathrm{Pd}$ for any Re_1 and Re_2, i.e., the curvature of the surface is constant and therefore the surface is a sphere whose radius R_0 is given by $(p_{cap} - p_\infty)$; then $2/R_0 = (p_{cap} - p_\infty)2a/\sigma$. The quantity $(p_{cap} - p_\infty)$ is determined from the condition that the volume of the drop is a

TABLE 1

Re_2	Re_1					Spherical bubble		Solid sphere
	0,4	20	40	60	100	[10]	[12]	[13]
	Cd							
0,1	238	—	—	236	—	160,5	161,6	240
1	25,2	—	—	24,12	—	16,8	17,6	26
12	3,58	—	2,5	—	2,47	2,2	2,2	3,9
40	1,78	—	1	0,93	—	0,8	0,83	1,9
60	1,5	—	—	0,71	—	0,66	0,6	1,6
100	1,28	0,67	—	0,52	—	0,48	0,4	1,2
200	1,13	0,65	—	—	—	0,32	0,2	0,82

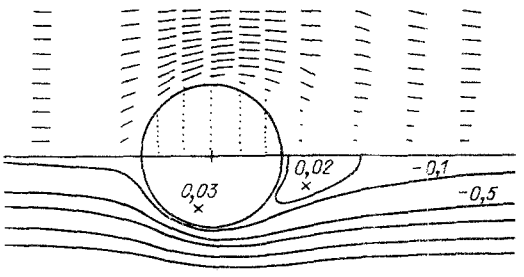

Fig. 1

constant. We choose this parameter such that $R_0 = 2$. This corresponds to introducing the unit of length $\ell = \sigma/2(p_{cap} - p_\infty)$ in place of a (for a sphere $\ell = a/2$ and the parameters Re_1, Re_2, We, and Fr are easily redefined in terms of ℓ). Calculations for deformed drops are carried out for fixed Re_1 and Re_2 and different values of the Weber number with a step-size δWe, beginning with We = 0 (the algorithm is discussed in [9]). For small Re_1 the solution can be compared with the result for flow around a solid sphere.

The large number of independent parameters complicates the interpretation of the numerical results and comparison with experiment. We use the parameters $R_\sigma = a/(\sigma/\rho_2 g)^{1/2}$, $R_\nu = a/(\nu_2^2/g)^{1/3}$. In the R_σ, R_ν plane the external liquid is represented as a straight line, since $(R_\sigma/R_\nu)^6 = \rho_2^3 g \nu_2^4/\sigma^3 = M$ (M is the Morton number of the external medium [11]). By plotting the basic parameter Fr on the R_σ, R_ν plane, the effect of the liquid making up the drop on its rise in the external liquid can be determined for different values of Re_1, Re_2, and We. The parameters are related to one another by the equations

$$R_\sigma = (We/2Fr)^{1/2},\quad R_\nu = (Re_2^2/4Fr)^{1/3},\quad M_d = \left(\frac{\rho_1}{\rho_2}\right)^3 \frac{2We^3}{Fr\,Re_1^4}. \tag{3.1}$$

4. Rise of Spherical and Slightly Deformed Drops. For We = 0 we hava a spherical drop with $R_0 = 2$ for any Re_1, Re_2. The boundary condition (2.4) is satisfied exactly, and the flow inside and outside the drop is found by solving the problem of a liquid flowing around a sphere. The parameter Fr is computed from the condition for steady motion, i.e., the drag force and buoyancy force on the drop are equal. Since the drag coefficient Cd is a basic hydrodynamic characteristic of a body moving in a fluid, we compute Cd for a rising drop: $Cd = (\rho_2 - \rho_1)Vg/(\rho_2 U^2/2)(\pi a^2) = (1 - \rho_1/\rho_2)8/3Fr$. It differs from Cd of a bubble [10] by the factor in parentheses due to the nonzero density of a drop. Here V is the volume. The usual value of Cd for a bubble is obtained by putting $\rho_1/\rho_2 = 0$.

The calculated values of Cd for different Re_1, Re_2 ($R_\sigma = 0.1$) are given in Table 1 for spherical drops. The values of Cd for $Re_1 = 0.4$ are within 9% of the values for flow around a solid sphere [13] for $Re_2 \leqslant 100$. At $Re_2 = 200$ the difference is 27%. We note that Cd is larger for a drop than for a solid sphere for $Re_2 = 100$, 200. The flow in the external liquid is continuous up to Re = 200 but for $Re_2 = 100$ and 200 there is a region of secondary flow behind the sphere which does not directly touch the surface of the drop (Fig. 1, $Re_1 = 0.4$, $Re_2 = 200$, Fr = 2.1; below: lines of constant stream function, above: the velocity field). Inside the drop and within the wake there are weak vortices rotating in the same direction. The local maxima of the stream function are 0.03 and 0.02, respectively. The external flow is the source of the vortex motion. The vortex inside the drop is induced by friction on the interface, while the external vortex is the result of the slowing of the liquid behind the drop. There is no separation of the flow from the surface, as in the case of a solid sphere [13], because the flows from the two vortices in the same direction must be matched on the surface of the drop. It is impossible to do this directly, since the velocity vector must be continuous across the surface. In order for the boundary of the secondary flow to pass out from the surface of the drop, we must have a third "buffer" vortex between the two vortices described above. This is possible if the vortex motion behind the drop is sufficiently strong, which can spread out the flow across part of the boundary and thereby generate a new counter flow inside the back of the drop. This process indeed occurs for sufficiently large We. The number of iterations required to compute the flow functions dramatically increases when We = 0.46 ($Re_1 = 0.4$, $Re_2 = 200$). Upon generation of a new vortex inside the drop the vortex outside the drop begins to move away, and a new vortex is formed, directly touching the surface of the drop. It increases in size until the flow again becomes steady (triangles in Fig. 3) or else the process will be unsteady. There is a jump in

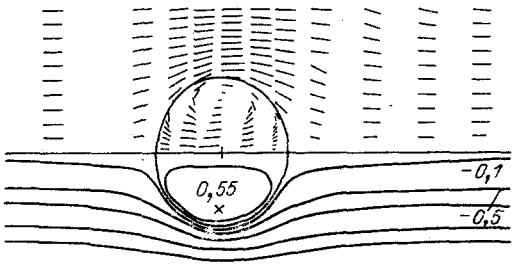

Fig. 2

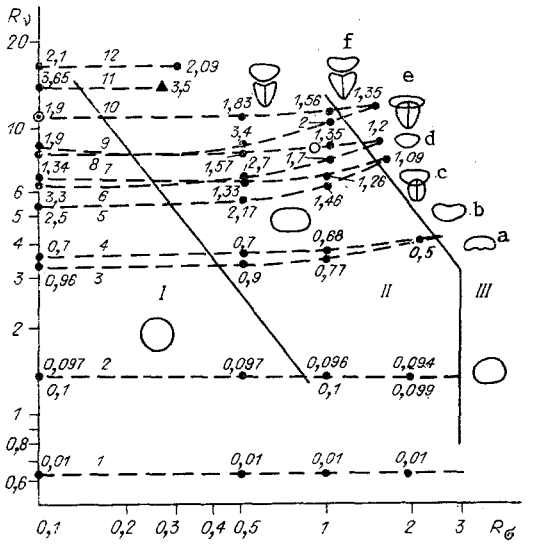

Fig. 3

the drag coefficient: Cd = 0.69, which is 16% smaller than Cd for a solid sphere [13] (before the transition Cd for the drop was 27% larger). The pressure over the outer surface of the drop varies significantly over the boundary, i.e., the force acting on the drop varies strongly in both magnitude and direction. This discussion obviously does not describe the evolution of the process in physical time, since it corresponds to evolution with respect to a fictitious time. But since one can often observe the rise of a light sphere in the form of a series of separate jerks, it gives indirect information on the possible processes.

Large Re_1 corresponds to the case when the drop is the less viscous medium. We see from Table 1 that for $Re_1 = 60$ the drag coefficient for $Re_2 > 1$ differs from Cd for a bubble by 8-12%. We see that for $Re_2 = 12$ the difference in Cd for $Re_1 = 40$ and 100 is very slight. Figure 2 illustrates the flow for $Re_1 = 60$, $Re_2 = 100$, We = 0.88 (Fr = 4.1, $R_\sigma = 0.33$, $R_\nu = 8.46$). The drop is slightly deformed and there is a strong Hill's vortex inside, whose center is near the boundary of the drop. The maximum values of the fluid velocity inside and outside the drop are approximately the same. The ratio of the velocities remains approximately the same for smaller values of Re_2 and We. As we increase Re_1 at fixed Re_2, the flow inside the drop changes from that shown in Fig. 2 to that shown in Fig. 1, where the liquid inside the drop is practically at rest. The stagnant region behind the drop disappears for $Re_1 = 20$ for slightly deformed drops.

Calculations for $Re_2 \leqslant 1$ show that Cd is approximately independent of Re_1. The flow is independent of the medium making up the drop. This is not surprising, since the Hill's vortex is an exact solution of the Navier–Stokes equations for small Re_2, independent of Re_1 [13]. For $Re_1 = 0.4$, $Re_2 = 0.1$, We = 0.0004 (Fr = 0.009, $R_\sigma = 0.15$, $R_\nu = 0.65$, $M = 1.4 \cdot 10^{-4}$, $M_d = 10^{-9}$) there is strong vortex motion inside the drop. These solutions correspond to rise of a liquid drop whose Morton number M_d is smaller than M for the external medium. The ratio M is the same as for $Re_2 > 1$, $Re_1 > 20$ (when $Re_1 = 0.4$ the value of M_d is larger than M of the external medium). For fixed Re_2, the value of M_d varies by more than seven orders of magnitude for $Re_1 = 0.4$-60. For example, for water $M \approx 10^{-11}$, for mineral oil $M \approx 0.01$, and for syrup (Bond) $M \approx 10^6$ [14].

5. Rise of Deformed Drops. As We increases the drop is deformed and it begins to flatten out in the plane perpendicular to its motion. The change in surface area reaches 3% (the ratio of the transverse and longitudinal dimensions of the drop) at We ≈ 0.24 for different Re_1 and $Re_2 \geqslant 1$. This is region I in the R_σ, R_ν plane (Fig. 3). For $Re_2 \leqslant 1$ the flow and the deformation of the boundary are constant for $0.4 \leqslant Re_1 \leqslant 60$, but for larger Re_2 there are significant differences. For example, the upper end of the straight line corresponding to the boundary of region I is shifted slightly to the right for $Re_1 = 0.4$ and We increases very slightly.

The dashed lines in Fig. 3 show the calculations for different We and fixed Re_1 and Re_2: 1) $Re_1 = 0.4$, $Re_2 = 0.1$ (identical to $Re_1 = 60$, $Re_2 = 0.1$); 2) 0.4 and 1 (practically identical to $Re_1 = 60$, $Re_2 = 1$); 3) 40 and 12, 4) 0.4 and 12; 5) 60 and 40; 6) 60 and 60; 7) 0.4 and 40; 8) 60 and 100; 9) 0.4 and 60; 10) 0.4 and 100; 11) 20 and 200; 12) 0.4 and 200.

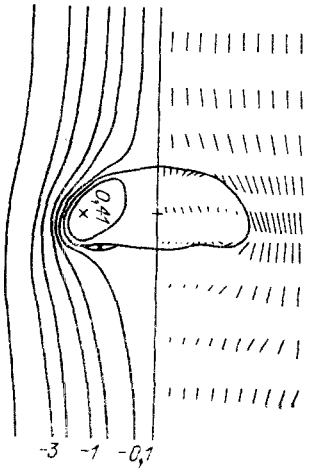

Fig. 4

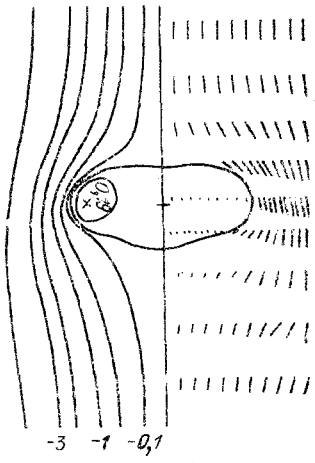

Fig. 5

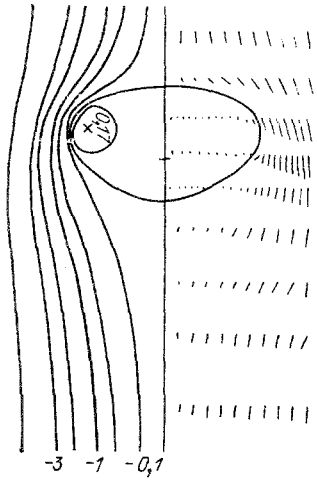

Fig. 6

The numbers labelling the points are the values of Fr obtained from the solution of the problem. We note the difference between this diagram and those of [9, 11], showing lines of constant Fr. The existence an additional independent parameter (the medium making up the drop) means that a large number of calculations are necessary to construct diagrams for a drop with a given M_d. The diagram of Fig. 3 obviously cannot easily be used to construct the dependence of the rise velocity of the drop on its radius in different liquids, but it shows the main effects of the rise process. For example, for fixed $Re_2 > 1$ and different Re_1 points corresponding to identical values of R_σ approach one another (curves 3 and 4; 5 and 7; 6 and 9; 8 and 10) as R_σ (and hence We) increases. The values of Fr also approach one another. This shows that the rise velocities of drops of the same size become equal in spite of the fact that the values of M_d corresponding to these curves differ by more than seven orders of magnitude. The shape of the drop changes from a sphere to an oblate spheroid on the right boundary of region II, shown by the broken line. The flow changes markedly.

For example, when $Re_2 \leqslant 1$ the curves corresponding to $Re_1 = 0.4$ and 60 are practically identical. The drop differs only slightly from a sphere and distortion in the back of the drop (flattening) and the appearance of a "corner" on the surface only become noticeable for $R_\sigma > 1$. For $Re_1 = 0.4$, $Re_2 = 1$, We = 1.62 ($R_\sigma = 2.94$, $R_\nu = 1.39$, M = 91, $M_d = 3.56$) a strong vortex exists inside the drop and the maximum velocity is comparable to the rise velocity. The drag coefficient is the same as for a solid sphere, while the flow inside the drop corresponds more to the case of a gas bubble (in this case $M_d < M$). The pressure p_2 on the surface resulting from the external flow increases monotonically as we move from the front to the back of the drop. For larger We (even for We = 1.6204, $R_\sigma = 3.18$) there is a change in the flow. The strength of the vortex inside the drop increases by nearly a factor of two and the velocity profile of the external flow becomes nonmonotonic over a cross section. The pressure is nonuniform near the corner, the boundary itself becomes wavy, Fr drops to 0.08, M = 106.6, $M_d = 4.16$. The boundary then oscillates and the flow becomes unsteady.

For $Re_2 \leqslant 0.1$ the flow characteristics are similar to the case $Re_2 = 1$, but the drop is nearly spherical. When $R_\sigma \geqslant 3$ steady flow does not exist and the boundary at the back of the drop oscillates from iteration to iteration in the calculation of the surface.

For $Re_2 > 1$ the rise velocity depends significantly on the medium making up the drop. With increasing deformation (increasing We) the dependence on the medium diminishes and practically disappears beyond a certain value of We (We ≈ 3.5-4.2 for $Re_2 = 12$-100). The inclined part of the broken line separating regions II and III in Fig. 3 corresponds to We ≈ 4-4.5. On the boundary either a turbulent wake appears behind the drop (for $Re_1 \geqslant 40$) or the boundary is wavy at the back of the drop (Fig. 4, $Re_1 = 40$, $Re_2 = 12$, We = 6.1, Fr = 0.45, $R_\sigma = 2.6$, $R_\nu = 4.3$, M = 0.049, $M_d = 3.9 \cdot 10^{-7}$). The flow passing around the drop is continuous and there is a strong vortex inside the drop whose center is near the drop boundary and whose velocity distribution is practically uniform over the drop cross section and much smaller than the rise velocity. With further increase of We the surface waviness is amplified and in the trough near the edge there is a stagnant zone (similar to what happens in the case of a bubble, see Fig. 3b of [11]; the external medium and the drop size are approximately the same). However, for a drop a broad turbulent wake does not form behind the drop,

as in the case of a bubble. The boundary near the back of the drop oscillates from iteration to iteration with further increase in We.

The solution for $Re_1 = 0.4$, $Re_2 = 12$ has the symmetric form of an oblate spheroid up to We = 3.4 ($R_\sigma = 1.9$). Even for We as small as 3.48 the number of iterations required to find the flow functions increases markedly and the surface of the drop becomes wavy (Fig. 5, Fr = 0.48, $R_\sigma = 1.91$, $R_\nu = 4.22$, M = 0.0086, $M_d = 6.2$) and steady flow is not possible. For large Re_2 the dependence of the drop deformation on We is similar up to We $\approx$ 3.45. For small Re_1 the drop has a flatter leading edge and becomes wedge-shaped. The flow is shown in Fig. 6 for $Re_1 = 0.5$, $Re_2 = 45$, We = 3.85 (Fr = 1.1, $R_\sigma = 1.32$, $R_\nu = 7.6$, $M = 2.6 \cdot 10^{-5}$, $M_d = 2.6$). Results for larger values of We could not be obtained: the surface of the back of the drop oscillated from iteration to iteration in the calculation of surface shape. For large Re_1 the drop shape is symmetric up to We = 3.45, becomes asymmetric for larger We, and beginning at We = 4.5 a turbulent wake is formed behind the drop in the external liquid and inside the drop another toroidal vortex is formed in the back of the drop rotating in the opposite direction. The three vortices form a system hydrodynamically consistent with the external flow and they are joined on the surface of the drop. Figure 7 shows the flow for $Re_1 = 69$, $Re_2 = 45$, We = 4.95 (Fr = 1.1, $R_\sigma = 1.5$, $R_\nu = 7.85$, $M = 5 \cdot 10^{-5}$, $M_d = 9.7 \cdot 10^{-9}$). As We increases the extent of the vortex flow in the external medium and inside the back of the drop increases.

For $Re_2 = 60$ the distance between curves 6 and 9 (corresponding to $Re_1 = 60$ and 0.4; see Fig. 3) increases. This implies that the medium making up the drop has a significant effect on the rise, in spite of the fact that the density ratio is the same. As We increases a zone of secondary flow (circles in Fig. 3) forms at a certain distance behind the drop (for $Re_1 = 0.4$). The vortex motion is weak both inside and outside the drop. The drop flattens out, the zone of secondary flow behind it increases, and a depression appears in the front part of the drop upon transition into region III. Flow with We = 4.62 (Fr = 1.19, $R_\sigma = 1.4$, $R_\nu = 9.1$, $M = 1.3 \cdot 10^{-5}$, $M_d = 6.58$) has the same structure as in Fig. 8. For $Re_1 = 60$ the shape remains symmetric until the formation of a vortex behind the drop (We = 4.55) and after with increasing We. For We = 4.97 (Fr = 1.22, $R_\sigma = 1.43$, $R_\nu = 9.02$, $M = 1.58 \cdot 10^{-5}$, $M_d = 1.55 \cdot 10^{-8}$) the flow is shown in Fig. 9. The pressure on the surface of the drop is practically symmetric about the $\theta = \pi/2$ axis.

For $Re_2 = 100$ the calculated flow near a spherical drop is different (curves 8 and 10 in Fig. 3). When $Re_1 = 0.4$ there is secondary flow behind the drop but not directly touching it, as in Fig. 1. The forward part of the drop flattens out with increasing We and the region of secondary flow behind it increases. A depression in the front of the drop appears for We $\approx$ 4.5. Figure 8 (We = 5.22, Fr = 1.37, $R_\sigma = 1.38$, $R_\nu = 12.19$, $M = 2.1 \cdot 10^{-6}$, M_d = 8.2) shows vortex motion behind the drop and the strength of this vortex exceeds that of the vortex inside the drop.

For $Re_1 = 60$ the flow is continuous and the shape of the drop is symmetric up to We $\approx$ 4.3. A closed turbulent wake appears at We = 4.34 (along with another vortex inside the back of the drop). As We increases the vortex behind the drop increases in size (Fig. 9, We = 5.56, Fr = 1.35, $R_\sigma = 1.43$, $R_\nu = 12.25$, $M = 2.6 \cdot 10^{-6}$, $M_d = 2 \cdot 10^{-8}$). Figures 8 and 9 illustrates the effect of the medium making up the drop on its rise and shape. The Morton numbers of the drop differ by more than seven orders of magnitude, while R_σ and R_ν are close, i.e., the external medium is practically the same in the two figures, as is the size of the drop. The rise velocities are the same, but the flow structures are very different.

6. Discussion of the Results. The types of flow obtained from the numerical solution of the Navier–Stokes equations are illustrated schematically in Fig. 3. Some explanation is required for the graphs in region III. For example a) corresponds to $Re_1 = 60$, b) $Re_1 = 0.4$; c) and d) $Re_2 = 12$; e) and f) $Re_2 = 100$ for curves 3 and 4 with the same correspondence of Re_1. These pairs of graphs show the type of surface shape for the Morton number of the drop within the given interval of M_d. For small Re_1 we have essentially a solid surface with a certain degree of elasticity, while for large Re_1 the results are close to the solution for a rising bubble and can be used as a model for a vapor bubble. The calculations for $Re_1 = 4$ and $Re_2 =$ 60 and 200 (small We) reflect the properties of a bubble to a greater degree than those of a solid particle. Inside the drop the maximum velocity is about half of the rise velocity of the drop and the region of secondary flow behind the drop is absent.

The inclined lines between regions I and II and between II and III are based on calculations with $Re_1 = 60$ and are close to the results for a bubble [11]. The values of Fr at

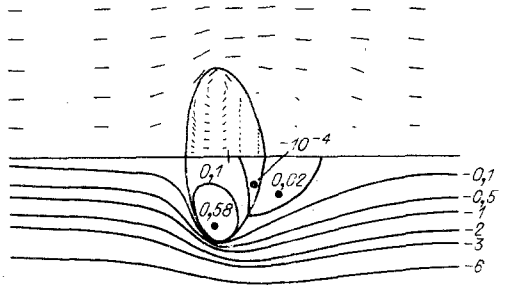

Fig. 7

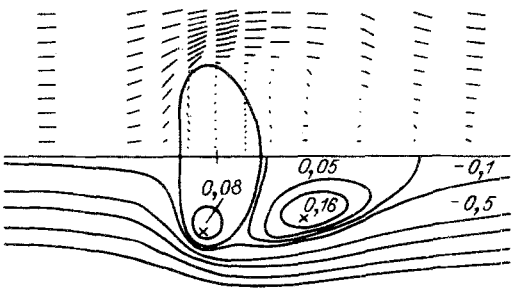

Fig. 8

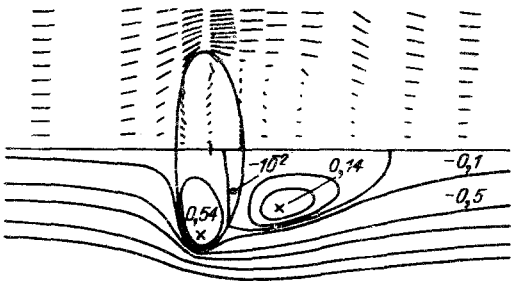

Fig. 9

corresponding points of Fig. 3 and Fig. 4 of [11] differ by about 20%; however, there are qualitative differences in the flow: in the case of a drop, there are unsteady oscillations of the surface for certain Re_1, Re_2 in region III, which result from the presence of matter inside the drop. A discontinuity across the drop can occur only when a new vortex is formed inside it. In order for this to be possible sufficiently strong vortex motion must exist in the stagnant zone behind the drop, capable of spreading the flow across part of the surface and creating the conditions for a new "buffer" vortex.

The curves for different valus of Re_1 and fixed Re_2 join when a depression occurs at the forward part of the drop ($Re_1 = 0.4$). At this point the rise velocity becomes self similar with respect to the medium making up the drop. It is not difficult to show that the lines Fr = const for a constant value of M_d have the same structure as for a bubble [11], and the inclined line between regions II and III in Fig. 3 passes near the points of contact of the lines representing the external medium with the lines of constant Fr. The size dependence of the rise velocity of a drop of a given liquid in another liquid has a local maximum preceding the formation of a turbulent wake behind the drop for external media with small M. For $M \sim 10^{-4}$-10^{-2} this dependence has an inflection point resulting from unsteady oscillations at the back of the drop. These features occur in the region $We \approx 4$-4.5. As shown by numerous experimental studies [8] surface oscillations of the drop are observed for these values of We.

As in the case of a rising bubble, the formation of a turbulent wake behind the drop leads to self-similar behavior of the rise velocity with respect to one of the hydrodynamic parameters: R_ν for small M ($M < 0.004$) and R_σ for larger M. Hence the formation of a vortex behind the drop (for small M_d) and the depression in the forward part of the drop (for M_d large compared to M) lead to self-similar behavior of the rise velocity with respect to both the medium making up the drop and one of the hydrodynamic parameters R_σ or R_ν. In region I (spherical drops) the rise velocity is self-similar with respect to R_σ, and for $Re_2 \leqslant 1$ it is also self-similar with respect to M_d.

For large Re_2 the drop rises along a curved path because of the formation of a turbulent wake behind the drop, which in liquids with low viscosity (small M) leads to a loss of stability of rectilinear motion. Surface-active matter and impurities on the surface of the drop lead to friction on the surface from the liquid flowing over it. The calculations with Re = 200 give a qualitative explanation of the unsteady processes accompanying the rise of bubbles in distilled water and in alcohol [14] (corresponding to the region near the local maximum in the rise velocity).

The maximum value of the velocity of the liquid inside the drop decreases (in comparison with the rise velocity of the drop) with increasing flattening of the drop (increasing We). Vortex motion is localized at the surface of the drop.

The solutions for $\rho_1/\rho_2 = 0.5$ give similar results for the surface deformation and flow structure. For the same Re_1, Re_2, and We the values of Fr are smaller than for the case $\rho_1 = 0.1$ [9], and the lines of constant Re_1, Re_2 lie above the corresponding lines in Fig. 3. Hence the entire diagram is shifted upward for $\rho = 0.5$. We see from (3.1) that solutions can be found for drops with larger M_d than for $\rho = 0.1$, assuming the same external medium.

Calculations were carried out for intermediate values of the basic parameters. Here all of the parameters significantly affect the rise of the drop up to the transition to self-similar solutions, where the rise velocity for a given density ratio ρ depends on a single hydrodynamic parameter.

Finally we note that an exact correspondence between our calculations and those of [6, 7] is not possible, since there the flow was studied for a given value of Fr. The basic types of flow reported in [7] are consistent with our solutions. The results given here and in [6, 7] (from solutions using a different set of dimensionless parameters) therefore give a complete picture of the hydrodynamic processes accompanying the rise of a drop.

LITERATURE CITED

1. J. Hadamard, "Mouvement permanent lent d'une sphere liquide et visquence dans une liquids visquens," C. R. Acad. Sci., 152, No. 25 (1911).
2. W. Rybczynski, "Über die fortschreitende Bewegung einer flussigen Kudel in einem zahen Medium," Bull. Inst. Acad. Sci. Cracovia Ser. A, No. 1 (1911).
3. T. D. Taylor and A. Acrivos, "Deformation and drag of a falling viscous drop at low Reynolds number," J. Fluid Mech., 18, No. 3 (1964).
4. A. E. Hamielec and A. I. Johnson, "Viscous flow around fluid spheres at intermeidate Reynolds numbers," Can. J. Chem. Eng., 40, No. 2 (1962).
5. Y. Nakano and C. Tien, "Creeping flow of a power-law fluid over a Newtonian fluid sphere," AIChE J, 14, No. 15 (1968).
6. V. Ya. Rivkind, "Steady motion of a viscous deformable drop," Zap. Nauk Semin. Leningr. Otd. Mat. Inst. Akad. Nauk SSSR, No. 84 (1979).
7. V. Ya. Rivkind, Hydrodynamics and Heat and Mass Transfer in a Drop, Author's abstract of candidate's dissertation Physical-Mathematical Sciences, Leningrad (1986).
8. A. L. Gonor and V. Ya. Rivkind, Dynamics of Drops [in Russian], Itogi Nauk Tekh., Ser. Mekh. Zhidk. Gaza, VINITI, Moscow (1982).
9. P. K. Volkov, "Rise of a liquid drop in a vertical tube filled with another liquid," in: Computer Simulation in Mechanics [in Russian], Siberian Branch of the Russian Academy of Sciences, Inst. of Theoretical and Applied Mechanics, 4(21), No. 5 (1990).
10. C. I. Christov and P. K. Volkov, "Numerical investigation of the steady viscous flow past a stationary deformable bubble," J. Fluid Mech., 158 (1985).
11. P. K. Volkov and E. A. Chinnov, "Steady rise of an isolated bubble in an infinite liquid," Zh. Prikl. Mekh. Tekh. Fiz., No. 1 (1990).
12. D. C. Brabston and H. B. Keller, "Viscous flows past spherical gas bubbles," J. Fluid Mech., 69, No. 1 (1975).
13. G. K. Batchelor, An Introduction to Fluid Mechanics, Cambridge University Press (1973).
14. W. L. Haberman and R. K. Morton, "An experimental study of bubbles moving in liquids," Proc. ASCE, 49, No. 387 (1954).